First-principles study of competing mechanisms of nondilute Li diffusion in spinel Li_{x}TiS_{2}

Jishnu Bhattacharya and Anton Van der Ven

Phys. Rev. B **83**, 144302 — Published 18 April 2011

DOI: 10.1103/PhysRevB.83.144302

First-principles study of competing mechanisms of non-dilute Li diffusion in spinel Li_xTiS_2

Jishnu Bhattacharya[1], Anton Van der Ven[2*]

[1] *Department of Mechanical Engineering*

[2] *Department of Material Science and Engineering*

University of Michigan, Ann Arbor, USA

Abstract

We report on a first-principles study of non-dilute Li diffusion in spinel Li_xTiS_2 with the aim of elucidating the role of crystal structure and chemistry on Li mobility in intercalation compounds used as electrodes in Li-ion batteries. In contrast to transition metal oxide spinels, where Li ions occupy tetrahedral interstitial sites, Li ions in spinel Li_xTiS_2 preferentially occupy octahedral sites. This makes spinel Li_xTiS_2 a useful model system to explore diffusion mechanisms in three-dimensional intercalation compounds with octahedral Li occupancy. Elementary Li hops between neighboring octahedral sites pass through intermediate tetrahedral sites. High coordination of these intermediate tetrahedral sites by octahedral sites causes the migration barrier to be sensitive to the local Li concentration and configuration. Kinetic Monte Carlo simulations predict diffusion mechanisms mediated by triple vacancies and divacancies, which

---

*Corresponding author. Tel.: +001 7346153843; fax: +001 7347634788; E-mail address: avdv@umich.edu

leads to a strong concentration dependence of the chemical diffusion coefficient. Insights from this study combined with those gathered in past first-principles studies of layered intercalation compounds indicate that crystal structures with activated states that are highly coordinated by Li sites will result in diffusion mechanisms mediated by vacancy clusters, producing a chemical diffusion coefficient that decreases with increasing Li composition.

I. Introduction

Much effort is currently devoted to understanding the properties of nano-structured electrodes for Li ion batteries [1-12], in large part because a reduction in electrode dimensions minimizes solid-state Li diffusion distances, thereby enabling high charge/discharge rates. Nano-structuring of electrode materials, however, lowers the volumetric and gravimetric energy density of the battery, as each electrochemically active crystallite must contact electronically conducting additives. Large electrode particles are therefore preferred when the aim is to maximize the overall energy density [13]. But maintaining high charge/discharge rate capabilities requires high Li diffusion coefficients to ensure rapid insertion/removal of Li from the interior of each electrode particle. The highest Li diffusion coefficients are typically achieved in intercalation compounds made up of a crystallographically rigid host that can accommodate Li ions in interstitial sites.

Although solid-state Li diffusion in large part determines rate capabilities, very little is understood about the role of crystal structure and chemistry on Li diffusion in intercalation compounds. This is due to the difficulty of unambiguously measuring Li diffusion coefficients in electrode materials. Electrochemical measurements of diffusion coefficients such as the potentiostatic and galvanostatic intermittent titration techniques (PITT and GITT) [14] rely on the

assumption that Li diffusion within the electrode particles is rate limiting compared to other kinetic processes within the electrolyte and at electrode/electrolyte interfaces. Furthermore, uncertainties in electrode particle dimensions and shapes can lead to large errors in estimated diffusion coefficients from PITT and GITT experiments. More targeted measurement techniques of Li mobility, such as nuclear magnetic resonance (NMR) [15-17], provide invaluable information about Li hop mechanisms, frequencies and migration barriers [18-20], but this information is difficult to link to diffusion coefficients appearing in Fick's first law, especially in non-dilute regimes where interactions among Li ions lead to complex correlations between successive Li hops. In spite of the uncertainties in measured diffusion coefficients, however, experiment has unambiguously revealed that the Li diffusion coefficients in many intercalation compounds exhibit a strong dependence on Li concentration, often varying by several orders of magnitude [21-24].

Preliminary first-principles studies of Li diffusion in non-dilute intercalation compounds have provided important insights about the role of crystallography on the concentration dependence of Li diffusion coefficients [25-28]. The calculation of diffusion coefficients using kinetic Monte Carlo simulations applied to first-principles lattice model Hamiltonians [26, 27, 29] have shown, for example, that Li diffusion in layered intercalation compounds such as Li_xCoO_2 and Li_xTiS_2 is mediated by a divacancy mechanism. The divacancy mechanism is responsible for a rapid decrease in the Li diffusion coefficient as the Li concentration increases above $x = 0.5$. Layered intercalation compounds are also susceptible to large contractions in the lattice parameter perpendicular to the transition metal oxide/sulfide slabs as the Li concentration is reduced below $x = 0.5$, causing a significant decrease in Li mobility [25-27]. A similar study of spinel $Li_{1+x}Ti_2O_4$, showed that Li diffusion over the tetrahedral sites of the three-dimensional spinel crystal

structure is mediated by a single vacancy mechanism and therefore has less of a concentration dependence than layered intercalation compounds[28]. The intermediate state for Li hops between adjacent tetrahedral sites is an octahedral site, which in the spinel crystal structure is only coordinated by the initial and final states of the hop. This crystallographic feature shields the activated state from other Li ions, thereby rendering the activation barrier less sensitive to Li concentration in spinel oxide host materials when Li occupies the tetrahedral sites.

The aim of the present study is to broaden our understanding of the role of crystal structure on the concentration dependence of Li diffusion coefficients in intercalation compounds. Here we focus on Li diffusion in Li_xTiS_2 having the spinel crystal structure. Although similar to spinel $Li_{1+x}Ti_2O_4$, the change in anion chemistry from oxygen to sulfur leads to a switch in site preference for the Li ions, with Li occupying octahedral sites at all Li concentrations in the Li_xTiS_2 compound as opposed to the tetrahedral sites in $Li_{1+x}Ti_2O_4$ (for $x < 0$). As is revealed by the present study, a simple shift from tetrahedral occupancy to octahedral occupancy in the same crystal structure can result in dramatic differences in diffusion mechanisms and the concentration dependence of the Li diffusion coefficient. Hops between adjacent octahedral sites in the spinel crystal structure must pass through an intermediate tetrahedral site, which is coordinated by four octahedral sites. The four-fold coordination renders migration barriers very sensitive to the local Li concentration and configuration. As a result, diffusion in spinel Li_xTiS_2 is mediated by triple vacancies and divacancies, which causes a rapid decrease of the Li diffusion coefficient with increasing Li concentration. This finding has relevance for disordered rocksalt $LiMO_2$ intercalation compounds [30-32] where the disorder of the transition metal ions can force the Li ions to occupy octahedral sites within the fcc oxygen sublattice. The present study also shows that Li diffusion in crystal structures having activated sites that are highly coordinated by other Li sites

will be mediated by vacancy clusters, which in general result in a decrease of the Li diffusion coefficient as the Li concentration reaches saturation.

II. Methods

Our approach to studying diffusion in intercalation compounds relies on three steps. The first step is to calculate the energies of a large number of Li-vacancy configurations over the interstitial sites of the TiS_2 host from first principles. We also calculate the migration barriers for Li hops in a variety of Li-vacancy configurations from first principles. In the second step, the configurational energies are used to parameterize coefficients of an effective Hamiltonian that allows us to predict the energy of the crystal for any Li-vacancy configuration. Finally, the effective Hamiltonian is subjected to (kinetic) Monte Carlo simulations to predict thermodynamic and kinetic properties.

The first-principles total energy calculations are performed with Density Functional Theory (DFT) as implemented in the Vienna Ab-initio Simulation Package (VASP) [33, 34] within the Generalized Gradient Approximation (GGA). The projector augmented wave method [35, 36] was used to model the core electrons. We use the nudged elastic band (NEB) method as implemented in VASP for calculations of energy barriers associated with a particular Li-hop.

Thermodynamic properties arise from excitations at the electronic and atomic scale at finite temperature. Configurational excitations due to the large number of ways of distributing Li and vacancies over the interstitial sites of the host constitute the most important contribution to the thermodynamic properties of intercalation compounds. Contributions from electronic and vibrational excitations are not as important in Li-intercalation compounds and are not considered

in the present study. We use the well-established Cluster Expansion method from alloy theory[37, 38] to construct an effective Hamiltonian that predicts the energy of the crystal as a function of configurational (dis)order of the material. Each of *M* available sites within the host can be occupied either by a Li-ion or a vacancy. This gives rise to 2^M possible configurations of Li ions and vacancies. Each site can be assigned an occupation variable (σ_i) which can take a value of +1 if it is occupied by Li or -1 if it is vacant. Hence, we can express any configuration over M available sites with an array of +1's and -1's ($\vec{\sigma} = \{\sigma_1,...,\sigma_i,...,\sigma_M\}$). On the same interstitial sites, we can define clusters or collections of sites of variable sizes (point, pair, triplet etc.). A cluster is attributed a cluster function (φ) which is a product of the occupation variables of the member sites.

$$\varphi_\alpha(\vec{\sigma}) = \prod_{i \in \alpha} \sigma_i \tag{1}$$

where α is the index for the particular cluster. It is mathematically proven that these cluster functions form a complete and orthonormal basis set in configuration space and any configuration-dependent quantity (formation energy in our case) can be expressed as an expansion of the cluster functions according to [37].

$$E(\vec{\sigma}) = V_0 + \sum_\alpha V_\alpha \cdot \varphi_\alpha(\vec{\sigma}) \tag{2}$$

The coefficients (V_i) in the cluster expansion (equation 2), are called Effective Cluster Interactions (ECI's). The expansion is rigorous, if all clusters of the crystal are included[37]. But with rare exceptions[39], the most important interactions are usually of short range and any practical cluster expansion must be truncated.

First-principles formation energies for different Li-vacancy configurations are used to parameterize the ECI of the cluster expansion through a least-squares fit. The quality of the fit is measured by the root mean square error (RMS) and its predictive capability is measured by a leave one out cross-validation (WCV) score[40]. We use a genetic algorithm to select the most important clusters in a truncated cluster expansion [41]. The resulting cluster expansion is then used in Monte Carlo (MC) simulations to predict finite temperature thermodynamic properties. We use grand canonical Monte Carlo (GCMC) to study the equilibrium properties and kinetic Monte Carlo (KMC) to study kinetic behavior.

The chemical diffusion coefficient (D) relates the Li flux to the concentration gradient according to Fick's first law. This material property can be expressed as a product of a thermodynamic factor (Θ) and the jump diffusion coefficient (D_J) [42].

$$D = \Theta D_J \tag{3}$$

The thermodynamic factor (Θ) is a measure of the deviation from the thermodynamic ideality and is defined according to [42]

$$\Theta = \frac{\partial\left(\frac{\mu_{Li}}{k_B T}\right)}{\partial \ln x} \tag{4}$$

In the dilute limit, Θ equals unity as the interactions between different Li ions are negligible. At stoichiometric compositions where Li-vacancy ordering is stable, Θ diverges, as the thermodynamic properties of an ordered phase deviate strongly from thermodynamic ideality. Θ

can be calculated as a function of concentration in Grand Canonical Monte Carlo simulations by tracking the fluctuations of the Li concentration around its average value [42].

The jump diffusion coefficient (D_J) measures the collective mobility of all the diffusing Li-ions and can be calculated at equilibrium using the following Kubo-Green expression [43, 44].

$$D_J = \frac{1}{2dt}\frac{1}{N}\left\langle \left[\sum_{i=1}^{N}\Delta\vec{R}_i(t)\right]^2 \right\rangle \tag{5}$$

Where d is the dimension of the interstitial sub-lattice (3 for Li_xTiS_2 spinel), t is time, N is the number of Li ions and $\Delta\vec{R}_i(t)$ is the displacement vector connecting the end points of the trajectory of the i^{th} Li ion.

The tracer diffusion coefficient (D^*) is another measure of diffusion that is a reflection of the mobility of the individual Li ions. D^* is defined according to,

$$D^* = \frac{1}{2dt}\frac{1}{N}\sum_{i=1}^{N}\left\langle \left[\Delta\vec{R}_i(t)\right]^2 \right\rangle \tag{6}$$

Displacement vectors $\Delta\vec{R}_i(t)$ of the Li ions can be generated in KMC simulations[45, 46] where Li hops through the crystal structure are simulated stochastically. The displacements are the summation of individual atomic hops and each of these hops occurs with frequencies that can be approximated with transition state theory according to [47]

$$\Gamma = \nu^* \exp\left(\frac{-\Delta E}{k_B T}\right) \tag{7}$$

where ν^* is the vibrational prefactor and ΔE is the activation barrier. Both the activation barrier and vibrational prefactor can be calculated from the first principles. The migration barrier (ΔE) in equation (7) is sensitive to the local environment (i.e. local state of Li-vacancy (dis)order), which needs to be accounted for within KMC simulations. The configuration dependence of the migration barriers can be described with cluster expansion techniques, either using a local cluster expansion or by introducing an additional sublattice for the activated states [26-28].

III. Results

A. Thermodynamics and site stability

The spinel form of Li_xTiS_2 has cubic symmetry and belongs to the $Fd\bar{3}m$ space group. The sulfur atoms form an fcc sub-lattice, while the titanium atoms occupy half of the available octahedral sites, designated 16d. The remaining octahedral sites, designated 16c, and half of the tetrahedral sites, designated 8a, are available interstitial sites for the intercalating Li-atoms. Figure 1 illustrates the spinel crystal structure and the available interstitial sites.

We constructed a cluster expansion describing the energy dependence on Li-vacancy configurations over the octahedral and tetrahedral sites of spinel Li_xTiS_2. To this end, we calculated the total energies of 159 symmetrically non-equivalent arrangements of Li and vacancies over the interstitial sites (both tetrahedral and octahedral) in super cells consisting of up to 4 primitive cells from first principles. Total energies were calculated within the PBE implementation of the generalized gradient approximation (GGA) to density functional theory (DFT) using the Vienna ab initio Simulation (VASP) package [33, 34]. The core states of Li, Ti and S were treated with the projector augmented wave (PAW) method [35, 36]. A uniformly dense grid

of k-points (equivalent to an 8×8×8 k-point grid in the primitive cell) was chosen for all these calculations based on a k-point convergence test.

The total energy calculations show that configurations with octahedral Li are lower in energy compared to configurations with tetrahedral occupancy at the same composition. Hence, Li prefers octahedral sites to the tetrahedral sites for all Li compositions between $x = 0$ and $x = 1$ in Li_xTiS_2. This behavior differs from the Li site preference in the oxide Ti-spinel [28, 48], where Li energetically prefers tetrahedral sites when the number of Li ions is less than or equal to the number of tetrahedral sites.

The coefficients of the cluster expansion for the configurational energy were fit to reproduce the formation energies of the 159 Li-vacancy configurations in spinel Li_xTiS_2, calculated with reference to delithiated spinel (TiS_2) and fully lithiated spinel ($LiTiS_2$) with Li filling all octahedral sites. The cluster expansion contains 30 Effective Cluster Interactions (ECI), including the empty cluster, 2 point clusters, 6 pair clusters, 7 triplet clusters and 14 quadruplet clusters. The cluster expansion has a weighted root mean square error of 1.75 meV and a weighted cross validation score of 6 meV per Li_xTiS_2 formula unit.

Thermodynamic properties of Li_xTiS_2 at finite temperature can be determined by subjecting the cluster expansion to Monte Carlo simulations. The open circuit voltage curve, for example, is related to the Li chemical potential within Li_xTiS_2 according to the Nernst equation

$$\Phi = -\left(\mu_{Li}^{cathode} - \mu_{Li}^{o}\right)/e \tag{8}$$

where $\mu_{Li}^{cathode}$ is the Li chemical potential in the cathode (spinel Li_xTiS_2 in this study), μ_{Li}^{o} is the Li chemical potential in the reference anode, taken to be metallic Li, and e is the charge of an electron.

Grand canonical Monte Carlo simulations enable the calculation of a chemical potential versus composition relationship, which can be used to predict a finite temperature voltage curve using Eq. 8. Figure 2 shows the calculated voltage curve of spinel Li_xTiS_2 at 300 K. For each temperature and chemical potential, averaging over the Li composition and grand canonical energy was performed over 3000 Monte Carlo passes following 1000 equilibration passes. The smooth variation of the voltage curve indicates solid solution behavior for the whole composition range. The solid solution behavior is observed experimentally [49, 50] and the calculated voltage curve, while systematically under predicted, qualitatively resembles the experimental voltage curve. The site occupancies at moderate temperature were also tracked in the Monte Carlo simulations: in spinel Li_xTiS_2, Li is predicted to occupy exclusively the octahedral sites at 300 K, consistent with the first-principles total energy calculations which predict a preference for octahedral occupancy over tetrahedral occupancy at all Li compositions between $x = 0$ and 1.

B. Elementary Li-hops and migration barriers

While DFT calculations and grand canonical Monte Carlo simulations applied to the cluster expansion predict that Li occupies octahedral sites, Li migration between octahedral sites follows a curved path that passes through a tetrahedral site as illustrated in Fig. 3; a direct hop between neighboring octahedral sites would require Li to squeeze between a pair of sulfur ions. Nudged elastic band calculations predict the intermediate tetrahedral site to be a local minimum. As a

result, a migrating Li ion can thermalize in the tetrahedral site before continuing on to an adjacent octahedral vacancy or hopping back to the original octahedral site it started from.

The end state energies as well as the migration barrier for a particular hop depend on the local arrangement of Li and vacancies, especially at non-dilute Li concentrations. This local environment dependence needs to be accounted for to accurately quantify non-dilute Li diffusion in spinel Li_xTiS_2. We can distinguish between three different configurations in the immediate surroundings of a migrating Li ion. The intermediate tetrahedral site of a hop has four nearest neighbor octahedral sites, one of which is initially occupied by the migrating Li. If only one of the remaining octahedral sites is vacant, the Li ion hops into an isolated vacancy as illustrated in Fig. 3(a). If two are vacant, the Li hops into a divacancy (Fig. 3(b)) and if all three are vacant, it hops into a triple-vacancy (Fig. 3(c)). The energy along the migration paths for the three local environments as determined with DFT based nudged elastic band calculations are illustrated in Fig. 3(d). The NEB calculations were performed in a cubic super cell consisting of 32 oxygen, 16 titanium and variable number of lithium ions in the nearest neighbor shell containing the hop while more distant octahedral lithium sites are fully occupied. As is clear from Fig. 3(d), the energy of the tetrahedral site is very sensitive to the number of occupied nearest neighbor octahedral sites. A hop into a single vacancy must overcome the highest migration barrier while a hop into a triple vacancy encounters the lowest migration barrier. For the single-vacancy hop (hollow green squares), the energy barrier is ~600 meV, while for the di-vacancy (filled black squares) and the triple-vacancy hops (filled red circles) they are lower having values of ~420 meV and ~290 meV respectively.

The results of Fig 3 illustrate a strong dependence of the migration barrier on the local Li configuration within the octahedral shell surrounding the intermediate tetrahedral site. In the calculation of these barriers, all octahedral Li sites beyond the nearest neighbor shell of the tetrahedral site were filled with Li. However, variations in Li concentration and configuration at larger distances from the migrating Li ion could also affect migration barriers. Fig 4b shows the calculated migration barriers for Li-hops from an octahedral site to a tetrahedral site (ΔE_{oct} as schematically illustrated in Fig. 4a) for the same three nearest neighbor Li configurations but having different Li concentrations and Li-vacancy configurations further away from the migrating Li. In Fig. 4b the hollow green squares correspond to single vacancy hops, the filled black squares correspond to divacancy hops and the filled red circles correspond to triple-vacancy hops. Fig. 4b clearly shows three distinct bands of migration barriers, each corresponding to a particular immediate hop-environment, with the lowest band of migration barriers corresponding to triple vacancy hops and the highest to single vacancy hops. There are some variations in barrier for different configurations at the same concentration and a more pronounced variation with concentration. The migration barriers for triple vacancy hops tend to decrease with increasing Li-content. Similarly, for divacancy hops (filled black squares), there is some configurational dependence as well as a Li composition dependence that is nevertheless weaker compared to the triple vacancy hops. The values of the migration barriers for the triple vacancy hop as well as their slight decrease with increasing Li concentration is consistent with NMR measurements of Li migration barriers in spinel Li_xTiS_2 [51]. This study reported measured migration barriers of 0.31 eV and 0.26 eV for $Li_{0.35}TiS_2$ and $Li_{0.6}TiS_2$ respectively, which, within the numerical accuracy of the DFT-supercell calculations are in reasonable agreement with calculated values in Fig. 4(b) for the triple vacancy hop mechanism.

Since the tetrahedral sites are local minima in the energy landscape, a migrating Li ion will typically thermalize there before continuing to an adjacent octahedral site. As is clear from Fig. 3(d), the barrier that a Li ion must overcome to migrate to a neighboring octahedral site is also very sensitive to the local Li configuration. Unlike the octahedral to tetrahedral barrier, though, these barriers are insensitive to the Li concentration and arrangement beyond the nearest neighbor octahedral shell. This is illustrated in Fig. 4c, which shows the concentration dependence of tetrahedral to octahedral barriers (ΔE_{tet} as schematically illustrated in Fig. 4a) for the single vacancy, divacancy and triple vacancy environments. While there are large differences for the three different local environments, the barriers for each local environment form distinct bands as a function of Li concentration, and the dashed lines represent the arithmetic mean of all the values within each band. The deviations from this mean value is not more than 20 meV in any band, which is less than the typical numerical error due to the use of a periodic supercell and due to k-point sampling errors.

The vibrational prefactors (ν^*) appearing in the hop frequency, Eq. (7), were calculated from first-principles within the local harmonic approximation. The dependence of the vibrational pre-factor on composition and hop-environment was found to be small. In the kinetic Monte Carlo simulations to be discussed in the next section, we used a different value for each hop direction: 3.1 THz for the octahedral to tetrahedral hops and 7.1 THz for the tetrahedral to octahedral hops.

C. Macroscopic Li Diffusion

The diffusion coefficient appearing in Fick's first law arises from the collective transport of many Li ions. At non-dilute concentrations, Li ions interact with each other as they migrate through the crystal, experiencing different local environments along their trajectories. These Li

trajectories can be sampled explicitly within kinetic Monte Carlo simulations, where each Li hop occurs with a frequency given by transition state theory, Eq. (7). The sampled trajectories can then be used to numerically evaluate the Kubo Green expressions for diffusion coefficients as described in Sec. II. To predict the dependence of Li diffusion coefficients on Li concentration, it is crucial that the kinetic Monte Carlo simulations accurately account for the equilibrium degree of short and long-range order (among the Li and vacancies) and the dependence of the migration barriers on local Li configuration.

Several approaches have been developed to treat the configuration dependence of migration barriers, typically relying on a local cluster expansion [26-28]. In spinel Li_xTiS_2, however, the configuration dependence of the migration barrier is primarily restricted to the first-nearest neighbor octahedral shell of the intermediate tetrahedral site. As is clear in Fig. 4c, the barrier to leave the tetrahedral site, ΔE_{tet}, depends only on the occupancy of the nearest neighbor octahedral shell (i.e. 250 meV for a triple vacancy hop, 100 meV for a divacancy hop and 20 meV for a single vacancy hop). Within a kinetic Monte Carlo simulation, ΔE_{tet} can therefore be determined by simply counting the number of Li ions in the nearest neighbor octahedral shell. The migration barrier for an octahedral to tetrahedral hop, ΔE_{oct}, depends more sensitively on Li concentration and configuration, but, as schematically illustrated in Fig. 4a, can be calculated as the sum of two terms: (i) the difference in energies between the tetrahedral and octahedral sites when occupied by the hopping Li ion, $\Delta E_{tet-oct}$, and (ii) the migration barrier to hop from the tetrahedral site to the initial octahedral site, ΔE_{tet}, which depends only on the Li configuration in the nearest neighbor octahedral shell. The difference in energy between the tetrahedral and octahedral sites, $\Delta E_{tet-oct}$, is calculated with the cluster expansion constructed in Section IIIA as

it describes the energy of the crystal as a function of the Li arrangement over the octahedral and tetrahedral sites of spinel Li_xTiS_2.

In the KMC simulations, we used 1000 Monte Carlo passes for equilibration and another 1000 for averaging the tracer and self diffusion coefficients. We used 100 initial configurations for each concentration and averaged the relevant quantities over these different ensemble runs.

The various diffusion coefficients described in Sec. II are plotted in Fig 5a. The curve represented by the hollow squares shows the variation of the tracer diffusion coefficient, D^*, while the curve with the solid green squares corresponds to the jump diffusion coefficient, D_J. Both D_J and D^* decrease monotonically with concentration, D_J having a slightly greater numerical value compared to D^*. The values of D^* and D_J range over seven orders of magnitude, varying from $\sim 10^{-9}$ cm^2/s at dilute Li concentrations to $\sim 10^{-16}$ cm^2/s as all octahedral sites become filled. Fig. 5b shows the thermodynamic factor Θ versus Li concentration, as calculated in the grand canonical Monte Carlo simulations. The thermodynamic factor is unity in the dilute limit, consistent with the fact that as $x \rightarrow 0$, interactions among Li-ions become negligible and the solid behaves as an ideal solution. It increases rapidly by an order of magnitude as the Li concentration increases above $x = 0$, ranging between 10 and 30 for most Li concentrations. Θ diverges close to the stoichiometric phase of the fully lithiated spinel where Li-ions fill all the octahedral sites. The product of Θ and the jump diffusion coefficient, D_J, yields the chemical diffusion coefficient D (filled red circles in Fig 5a). D is numerically identical to D_J in the dilute limit, as Θ is unity there. Near this dilute limit, D increases with Li concentration due to the increase in Θ. However D_J drops much more rapidly than the increase in Θ with Li concentration x, resulting in a substantial drop of the chemical diffusion coefficient

as Li is added to the host. Near the fully-lithiated limit, the rapid increase in Θ causes D to drop at a slower rate than D_J. The chemical diffusion coefficient varies between ~10^{-8} cm^2/s to ~ 10^{-14} cm^2/s.

More insight about the strong concentration dependence of D^* and D_J can be gained from an analysis of the relative frequency of triple, di and single vacancy hops. This is illustrated in Fig. 6a, which shows that at low to intermediate concentrations, most hops are mediated by triple vacancies. Only at high Li concentrations do divacancy hops dominate, with a very small fraction of hops occurring into single vacancy environments at very high Li concentrations. The concentration dependence of the hop mechanism arises from a variation in the availability of triple, di and single vacancy clusters with Li concentration. Fig. 6b shows conditional probabilities that a Li atom will be surrounded by a triple vacancy, a divacancy and a single vacancy. These were calculated with grand canonical Monte Carlo simulations. At low Li concentrations where the vacancy concentration is large, Li ions are surrounded primarily by triple vacancies. As the Li concentration increases though, the fraction of triple vacancies drops off, with an increase in divacancy clusters at intermediate Li concentration. At high Li concentrations, Li ions are surrounded for the most part by single vacancy environments.

Although the availability of triple vacancies drops off rapidly as x approaches 0.5, the majority of hops still proceed with a triple vacancy mechanism at intermediate Li concentrations. This is due to the fact that the migration barrier for a triple vacancy hop is significantly lower than that for hops into divacancies, which are nevertheless more abundant at intermediate concentrations. Only at high Li concentrations where the number of triple vacancies becomes very small, do more hops occur into divacancies than into triple vacancies. The high migration barrier

associated with hopping into an isolated vacancy makes this mechanism unfavorable even at the highest Li concentrations. The strong concentration dependence of the diffusion coefficient, therefore, arises from a decrease in the concentration of triple vacancies and then of divacancies. There is also a rapid drop in the diffusion coefficient as the diffusion mechanism transitions from one mediated by triple vacancies to one mediated by divacancies, since the migration barrier for the latter is almost twice as large.

The concentration dependence of the diffusion coefficient is not only affected by the availability of vacancy clusters and their associated migration barriers. It can also be strongly affected by the efficiency with which the migration of vacancy clusters redistribute Li ions throughout the crystal. A convenient metric for the efficiency of diffusion is the correlation factor, *f*, which measures the deviation of the tracer diffusion coefficient (*D**) from what it would be if all successive Li-hops were uncorrelated (i.e., random walk). Mathematically the correlation factor can be calculated according to

$$f = \frac{\left\langle \Delta \vec{R}_i(t)^2 \right\rangle}{na^2} \tag{8}$$

where, $\Delta \vec{R}_i(t)$ is the displacement of a particular Li ion in time *t*, *n* is the number of hops and *a* is the hop distance. In the dilute limit, successive hops of the sparsely distributed Li ions will be largely uncorrelated and the correlation factor tends to unity. At the other extreme when *x* approaches 1 and the number of vacancies becomes very dilute correlations between successive Li hops become significant. Fig. 7 shows the calculated correlation factor for Li diffusion as a function of Li concentration. The correlation factor drops rapidly as Li is added to the crystal and is almost two orders of magnitude less than unity at high Li concentration. Cleary diffusion

mediated by triple vacancies and divacancies is highly correlated and thus inefficient in transporting Li.

IV. Discussion and Conclusion

While it is generally assumed that an increase in the dimensionality of the interstitial network of an intercalation compound will increase guest ion mobility, the present study has shown that this is not necessarily true and that the diffusion coefficient and its concentration dependence can be very sensitive to the crystal structure of the host. We have found in particular that vacancy clusters (as opposed to isolated vacancies) will mediate Li diffusion in intercalation compounds if more than two Li-sites coordinate the intermediate site of a Li hop (i.e. sites in addition to the end states of the hop). The preference for a vacancy cluster mechanism in those crystal structures has its origin in the strong dependence of the migration barrier on the Li occupancy of the neighboring sites immediately adjacent to the activated site: the barrier is low when all adjacent sites are empty (i.e. for a vacancy cluster) and increases significantly as the sites adjacent to the activated site become occupied by Li due to short-range Li-Li repulsion. This was already predicted for layered intercalation compounds [26, 27], where three octahedral sites coordinate the intermediate tetrahedral site that a Li must pass through when hopping between a pair of octahedral sites. In the layered intercalation compounds, a hop into a divacancy has a lower migration barrier than the same hop into an isolated vacancy. In fact the difference in migration barriers is so large that divacancies mediate diffusion over the whole composition range in layered intercalation compounds, even at high Li concentrations where the divacancy concentration vanishes. In spinel Li_xTiS_2, where Li ions occupy octahedral sites, this preference for hops into vacancy clusters becomes even more pronounced as the octahedral Li sublattice has

increased from two to three dimensions. Now four octahedral sites coordinate the intermediate tetrahedral sites, giving rise to triple vacancy hops in addition to divacancy and isolated vacancy hops.

Diffusion mediated by vacancy clusters results in a strong dependence of the diffusion coefficient on Li concentration since the concentration of vacancy clusters decreases with Li concentration. Furthermore, vacancy clusters are inefficient at redistributing Li ions throughout the crystal, especially at high Li concentration. This was found to be the case in layered Li_xCoO_2, where the correlation factor, *f*, drops rapidly as Li is added to the host and is very low at high Li concentration [26]. The same is predicted in the present study for Li diffusion in spinel Li_xTiS_2 mediated by both triple and divacancies. In spinel Li_xTiS_2, the correlation factor is of the order of 10^{-2} at high Li concentration. This is in stark contrast to spinel $Li_{1+x}Ti_2O_4$ for $x < 0$, where Li diffusion over tetrahedral sites occurs with a single vacancy mechanism and the correlation factor is significantly higher, having a value around 0.5 as the tetrahedral sites become saturated with Li ions [28].

One advantage of three-dimensional intercalation hosts such as spinel over layered ones is that the lattice parameter variations with Li concentration are less pronounced in the former. Migration barriers, in addition to being very sensitive to the local Li-concentration and environment, can vary strongly with lattice parameters. This is true in layered intercalation compounds where the migration barriers have been found to increase substantially due to the contraction in the lattice parameter *c*, perpendicular to the Li layers upon Li removal [26, 27]. This causes a reduction in the Li diffusion coefficient at low Li concentration in layered intercalation compounds. The cubic spinel lattice parameters are less sensitive to Li concentration than in

layered intercalation compounds. Hence the primary origin of the strong concentration dependence of the Li diffusion coefficient in spinel $LiTiS_2$ is the concentration dependence of triple and di-vacancy content. This leads to a monotonic decrease of the diffusion coefficient with increasing Li concentration.

The results of the present study are relevant for rock-salt type intercalation compounds with disordered transition metal cations over the octahedral sites of an fcc oxygen sublattice. Disordering of transition metals will produce a three-dimensional (although disordered) interstitial network for the Li ions with Li ions likely occupying octahedral sites as occurs in most transition metal oxides. While tetrahedral occupancy is observed in oxide spinels and transition metal oxides with local spinel-like environments [52], this site preference appears to arise from electrostatic effects peculiar to the cation ordering in spinel [28]. The present study indicates that increasing the dimensionality of the Li interstitial network by disordering of the transition metal cations will not necessarily increase the Li mobility at high Li concentration but rather introduce a strong concentration dependence of the Li diffusion coefficient.

Crucial in minimizing the concentration dependence of the Li diffusion coefficient is the use of a crystal structure in which the intermediate state of elementary Li hops has a low coordination by other Li sites. In this vein, high diffusion coefficients with negligible concentration dependence may be achievable in intercalation compounds with one-dimensional interstitial networks such as olivine[53]. Choosing crystal structures with activated states that are minimally coordinated by Li sites suppresses the tendency for diffusion mechanisms mediated by vacancy clusters, thereby eliminating a major cause of a strong concentration dependence of the Li diffusion coefficient. Additional considerations in minimizing the concentration dependence of the diffusion

coefficient include the use of crystal structures that undergo minor variation in lattice parameters with Li concentration [26, 27] and that shield the activated state from transition metal cations that can shift valence with Li concentration thereby resulting in strong migration barrier variations due to shifts in electrostatic interactions [26, 28].

Acknowledgement

The authors acknowledge financial support from DOE BES: EFRC Northeastern Center for Chemical Energy Storage DESC0001294 and TERAGRID for computational resources.

References

1 J. Maier, Nature Materials **4**, 805 (2005).

2 A. S. Arico, P. Bruce, B. Scrosati, J. M. Tarascon, and W. Van Schalkwijk, Nature Materials **4**, 366 (2005).

3 M. Wagemaker, W. J. H. Borghols, and F. M. Mulder, Journal of the American Chemical Society **129**, 4323 (2007).

4 N. Meethong, H. Y. S. Huang, S. A. Speakman, W. C. Carter, and Y. M. Chiang, Advanced Functional Materials **17**, 1115 (2007).

5 N. Meethong, H. Y. S. Huang, W. C. Carter, and Y. M. Chiang, Electrochemical and Solid State Letters **10**, A134 (2007).

[6] P. Gibot, M. Casas-Cabanas, L. Laffont, S. Levasseur, P. Carlach, S. Hamelet, J. M. Tarascon, and C. Masquelier, Nature Materials **7**, 741 (2008).

[7] C. Delmas, M. Maccario, L. Croguennec, F. Le Cras, and F. Weill, Nature Materials **7**, 665 (2008).

[8] M. Wagemaker, F. M. Mulder, and A. Van der Ven, Advanced Materials **21**, 2703 (2009).

[9] A. Van der Ven and M. Wagemaker, Electrochemistry Communications **11**, 881 (2009).

[10] B. Kang and G. Ceder, Nature **458**, 190 (2009).

[11] K. T. Lee, W. H. Kan, and L. F. Nazar, Journal of the American Chemical Society **131**, 6044 (2009).

[12] R. Malik, D. Burch, M. Bazant, and G. Ceder, Nano Letters **10**, 4123 (2010).

[13] W. Lai, C. K. Erdonmez, T. F. Marinis, C. K. Bjune, N. J. Dudney, F. Xu, R. Wartena, and Y. M. Chiang, Advanced Materials **22**, E139.

[14] C. J. Wen, B. A. Boukamp, R. A. Huggins, and W. Weppner, Journal of the Electrochemical Society **126**, 2258 (1979).

[15] M. Wilkening and P. Heitjans, Solid State Ionics **177**, 3031 (2006).

[16] C. P. Grey and N. Dupre, Chemical Reviews **104**, 4493 (2004).

[17] M. Wagemaker, A. P. M. Kentgens, and F. M. Mulder, Nature **418**, 397 (2002).

[18] M. Wilkening, W. Kuchler, and P. Heitjans, Physical Review Letters **97** (2006).

[19] M. Wilkening, R. Amade, W. Iwaniak, and P. Heitjans, Physical Chemistry Chemical Physics **9**, 1239 (2007).

[20] M. Wilkening and P. Heitjans, Physical Review B **77** (2008).

[21] K. Kanehori, F. Kirino, T. Kudo, and K. Miyauchi, Journal of the Electrochemical Society **138**, 2216 (1991).

[22] Y. I. Jang, B. J. Neudecker, and N. J. Dudney, Electrochemical and Solid State Letters **4**, A74 (2001).

[23] J. Barker, R. Pynenburg, R. Koksbang, and M. Y. Saidi, Electrochimica Acta **41**, 2481 (1996).

[24] J. M. McGraw, C. S. Bahn, P. A. Parilla, J. D. Perkins, D. W. Readey, and D. S. Ginley, Electrochimica Acta **45**, 187 (1999).

[25] A. Van der Ven and G. Ceder, Journal of Power Sources **97-8**, 529 (2001).

[26] A. Van der Ven, G. Ceder, M. Asta, and P. D. Tepesch, Physical Review B **64** (2001).

[27] A. Van der Ven, J. C. Thomas, Q. C. Xu, B. Swoboda, and D. Morgan, Physical Review B **78** (2008).

[28] J. Bhattacharya and A. Van der Ven, Physical Review B **81**.

[29] A. Van der Ven, H. C. Yu, G. Ceder, and K. Thornton, Progress in Materials Science **55**, 61.

[30] M. N. Obrovac, O. Mao, and J. R. Dahn, Solid State Ionics **112**, 9 (1998).

[31] W. Li, J. N. Reimers, and J. R. Dahn, Physical Review B **46**, 3236 (1992).

[32] C. S. Johnson, N. C. Li, C. Lefief, and M. M. Thackeray, Electrochemistry Communications **9**, 787 (2007).

[33] G. Kresse and J. Furthmuller, Computational Materials Science **6**, 15 (1996).

[34] G. Kresse and J. Furthmuller, Physical Review B **54**, 11169 (1996).

[35] P. E. Blochl, Physical Review B **50**, 17953 (1994).

[36] G. Kresse and D. Joubert, Physical Review B **59**, 1758 (1999).

[37] J. M. Sanchez, F. Ducastelle, and D. Gratias, Physica A **128**, 334 (1984).

[38] D. deFontaine, Solid State Physics - Advances in Research and Applications, Vol 47 **47**, 33 (1994).

[39] D. B. Laks, L. G. Ferreira, S. Froyen, and A. Zunger, Physical Review B **46**, 12587 (1992).

[40] A. van de Walle and G. Ceder, Journal of Phase Equilibria **23**, 348 (2002).

[41] G. L. W. Hart, V. Blum, M. J. Walorski, and A. Zunger, Nature Materials **4**, 391 (2005).

[42] R. Gomer, Reports on Progress in Physics **53**, 917 (1990).

[43] P. M. Richards, Physical Review B **16**, 1393 (1977).

[44] G. Mazenko, J. R. Banavar, and R. Gomer, Surface Science **107**, 459 (1981).

[45] A. B. Bortz, M. H. Kalos, and J. L. Lebowitz, Journal of Computational Physics **17**, 10 (1975).

[46] F. M. Bulnes, V. D. Pereyra, and J. L. Riccardo, Physical Review E **58**, 86 (1998).

[47] G. H. Vineyard, Journal of Physics and Chemistry of Solids **3**, 121 (1957).

[48] M. Wagemaker, A. Van Der Ven, D. Morgan, G. Ceder, F. M. Mulder, and G. J. Kearley, Chemical Physics **317**, 130 (2005).

[49] S. Sinha and D. W. Murphy, Solid State Ionics **20**, 81 (1986).

[50] V. Bodenez, L. Dupont, M. Morcrette, C. Surcin, D. W. Murphy, and J. M. Tarascon, Chemistry of Materials **18**, 4278 (2006).

[51] C. Prigge and W. Mullerwarmuth, Zeitschrift Fur Physikalische Chemie-International Journal of Research in Physical Chemistry & Chemical Physics **189**, 153 (1995).

[52] A. Van der Ven and G. Ceder, Electrochemistry Communications **6**, 1045 (2004).

[53] D. Morgan, A. Van der Ven, and G. Ceder, Electrochemical and Solid State Letters **7**, A30 (2004).

FIG 1: Crystal structure of TiS_2 spinel. (a) Stacking of transition metal octahedrons (b) The interstitial tetrahedral Li sites form a diamond network. Halfway in between two nearest neighbor tetrahedral sites, there is one octahedral Li site.

FIG 2: Calculated voltage curve for Li_xTiS_2 spinel as a function of Li composition.

FIG 3: Different nearest neighbor hop mechanisms and energy along the hop path in Li_xTiS_2 spinel. Atomic arrangements around (a) a single vacancy hop (b) a divacancy hop and (c) a triple vacancy hop. Only the relevant nearest neighbor shell around a tetrahedral Li site has been shown. The Ti atoms are omitted for the sake of clarity. (d) Energy along the migration path for three different hop mechanisms. The curves marked by the letters a, b and c correspond to the hop mechanism shown in (a), (b) and (c), respectively. The migration energies are calculated with nudged elastic band calculations where all further lithium sites are fully occupied except the nearest neighbor shell, where the number of Li atoms varies in the three different hop mechanisms.

FIG 4: (a) Schematic of the energy as Li migrates between neighboring octahedral sites passing through an adjacent tetrahedral site. (b) Migration barriers for Li hops from an octahedral site into an adjacent tetrahedral site, ΔE_{Oct}. (c) Migration barriers for Li hops from a tetrahedral site to an adjacent octahedral site, ΔE_{Tet}. Red circles correspond to triple vacancy hops, filled black squares to divacancy hops and the empty green squares to single vacancy hops.

FIG 5: (a) Diffusion coefficients as functions of Li concentration. Empty squares, filled green squares and filled red circles represent tracer diffusion coefficient (D^*), jump diffusion

coefficient (D_J) and chemical diffusion coefficient (D), respectively. (b) Variation of thermodynamic factor with Li composition.

FIG 6: (a) Relative frequency of different hop mechanisms sampled in the kinetic Monte Carlo simulations. (b) Relative abundance of single, di and triple vacancy clusters around Li atoms as calculated in grand canonical Monte Carlo simulations.

FIG 7: Variation of the correlation factor with Li composition.

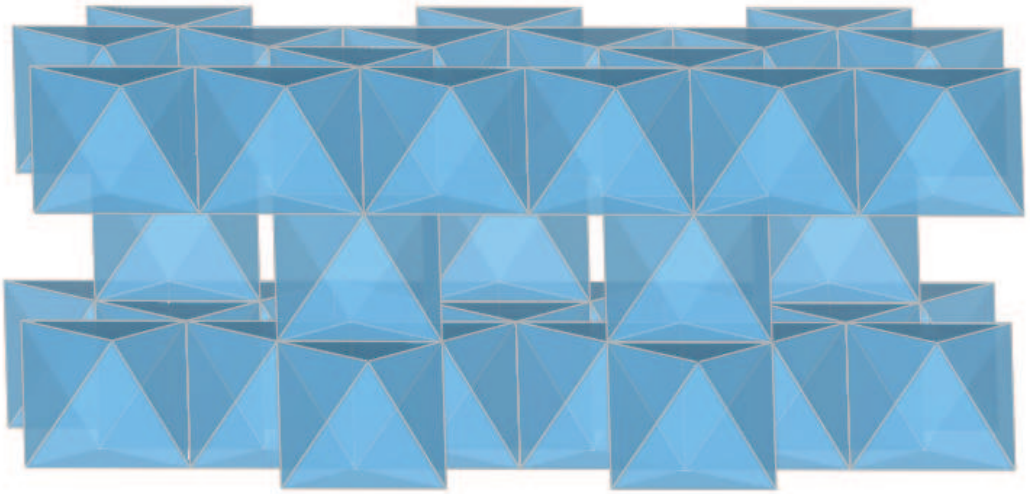

(a)

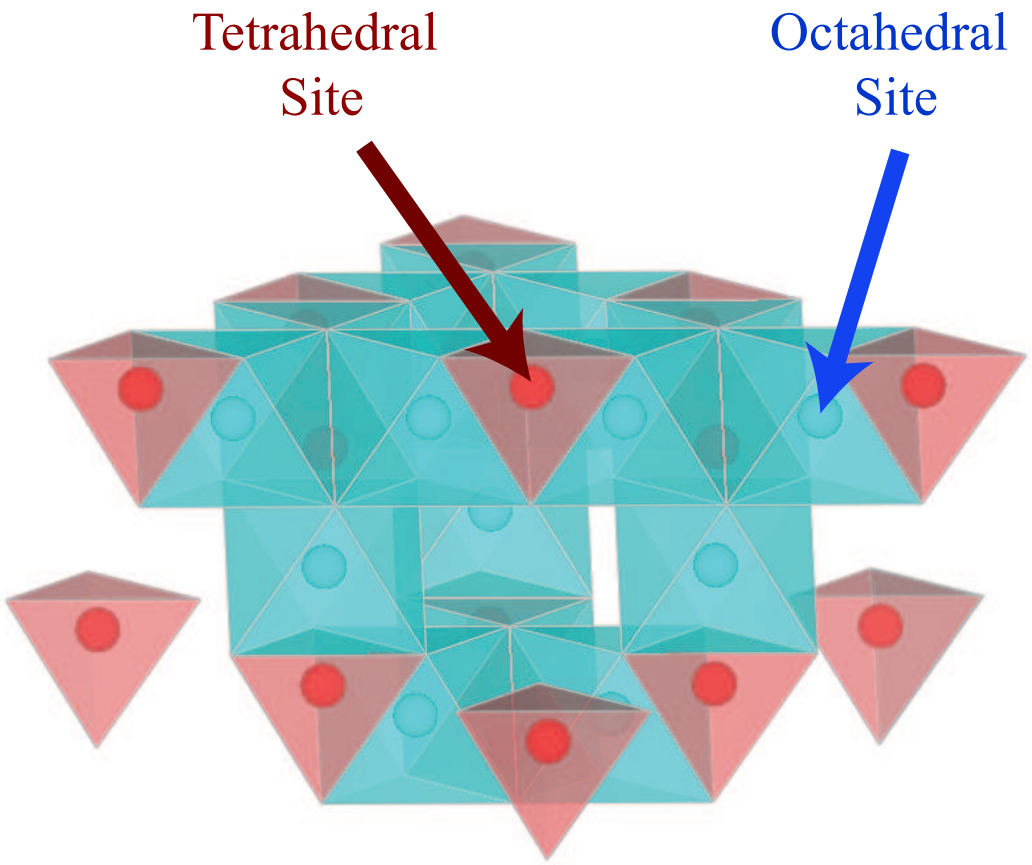

(b)

Figure 1 BY11342 03FEB2011

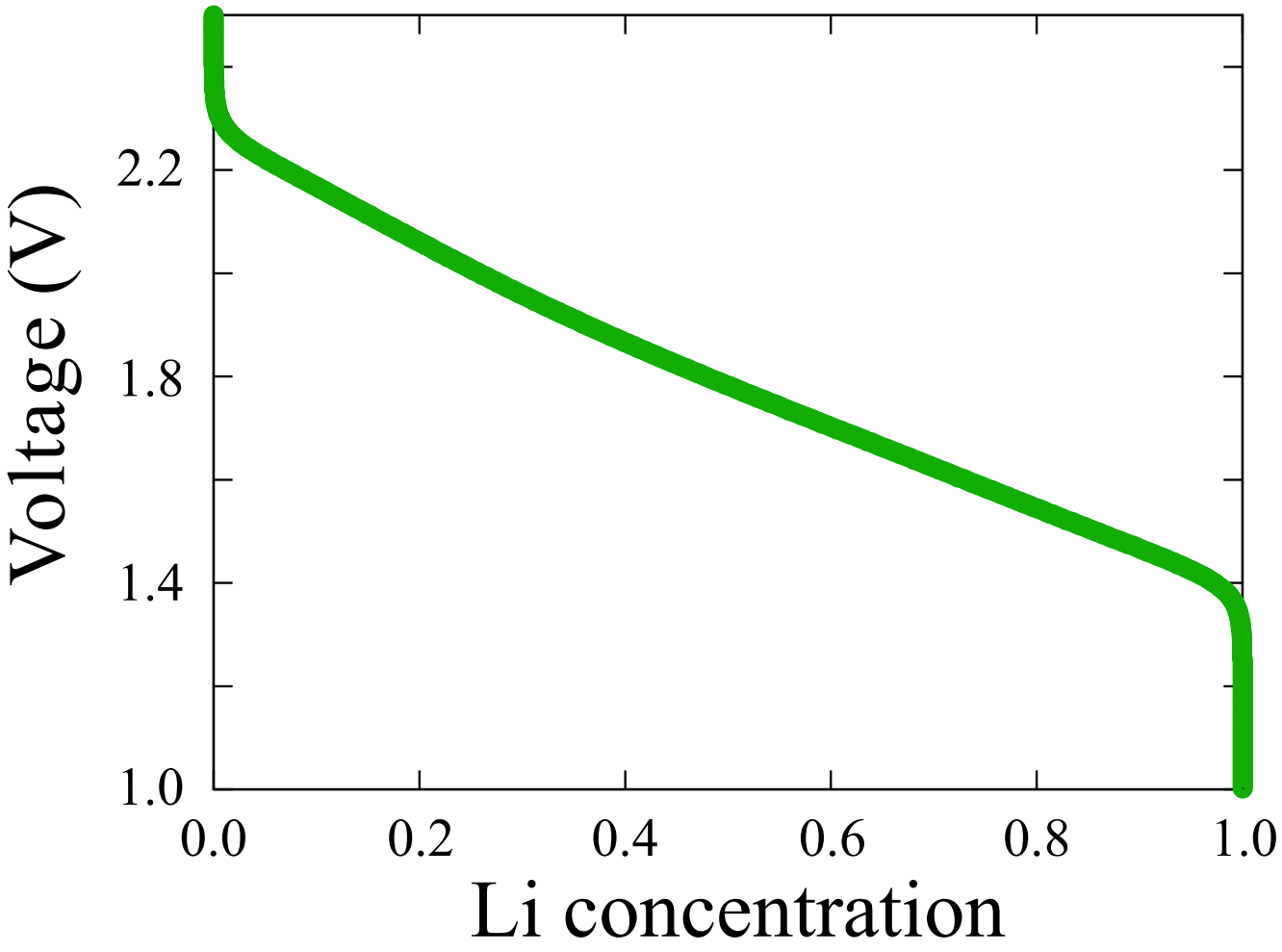

Figure 2 BY11342 03FEB2011

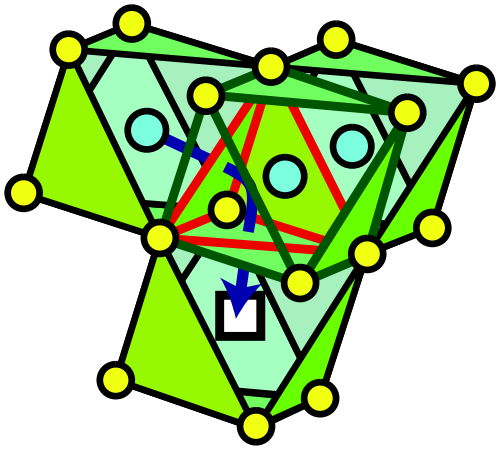

(a)

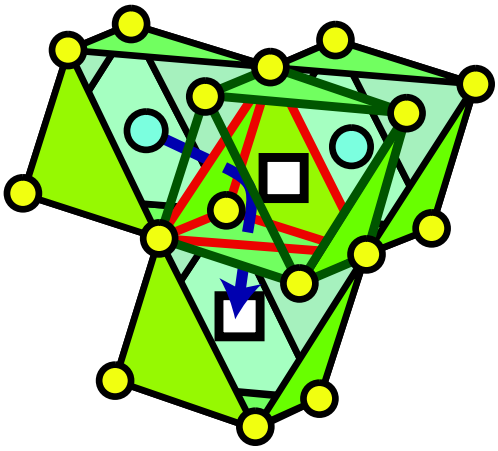

(b)

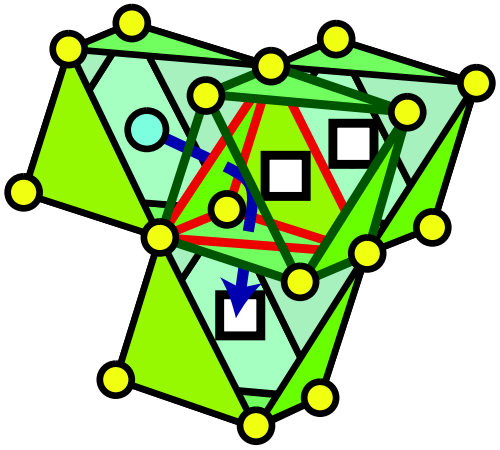

(c)

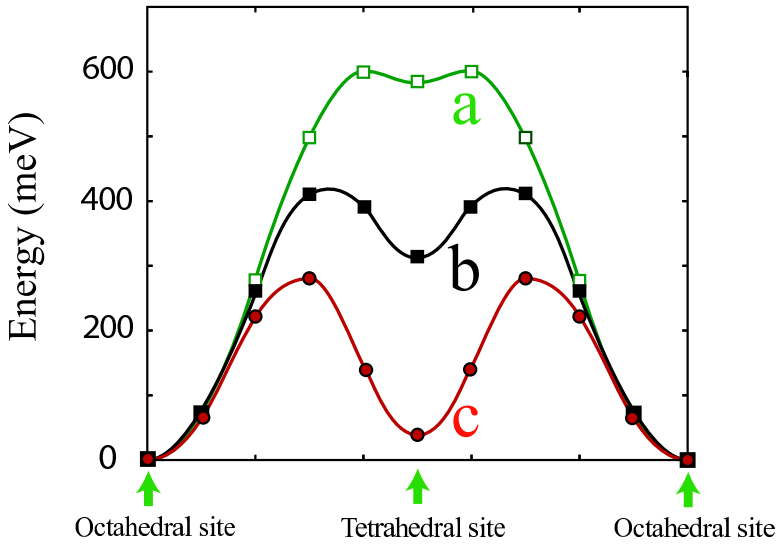

(d)

Figure 3 BY11342 03FEB2011

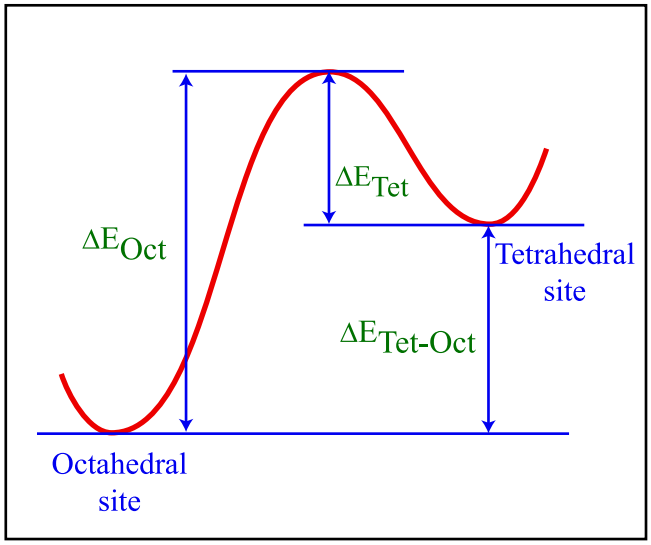

(a)

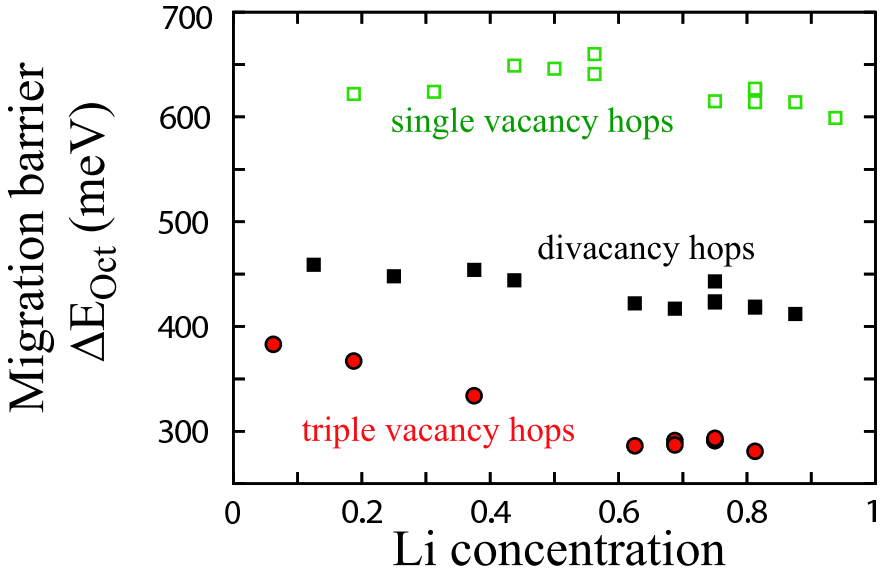

(b)

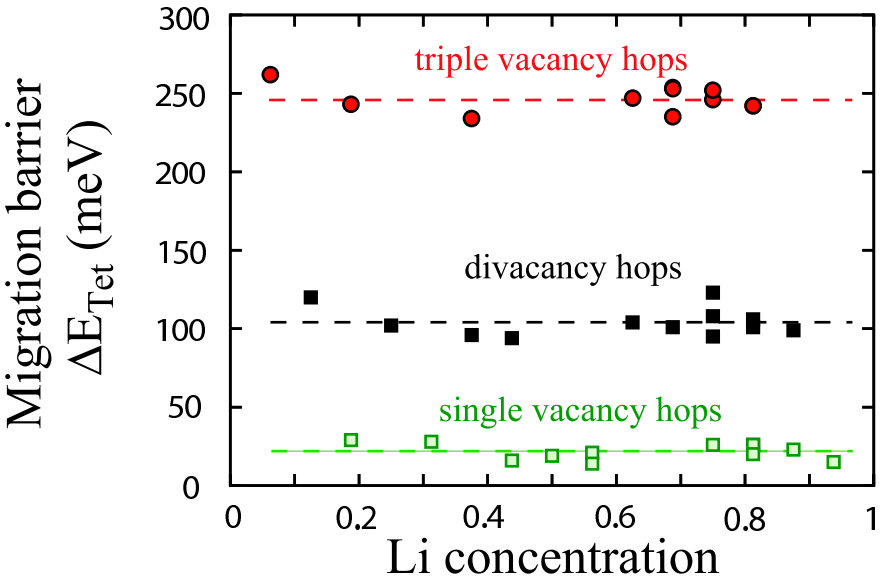

(c)

Figure 4 BY11342 03FEB2011

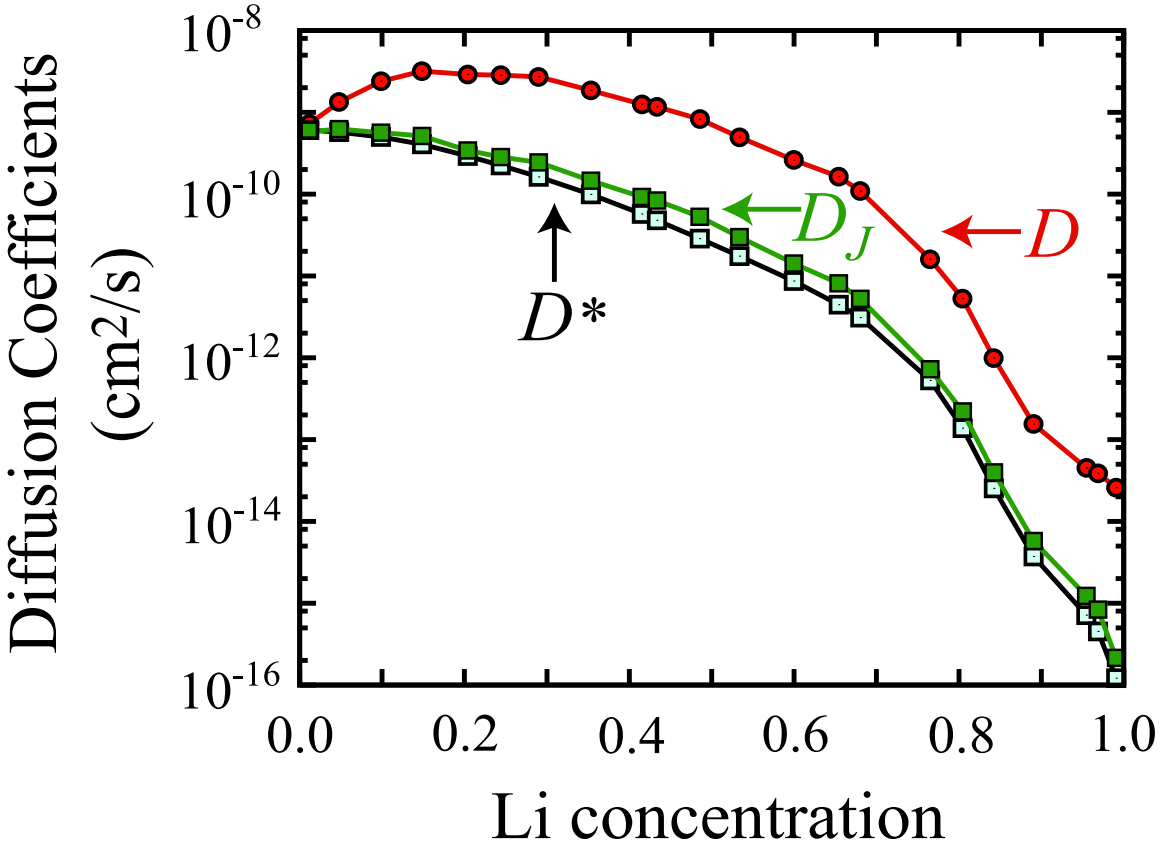

(a)

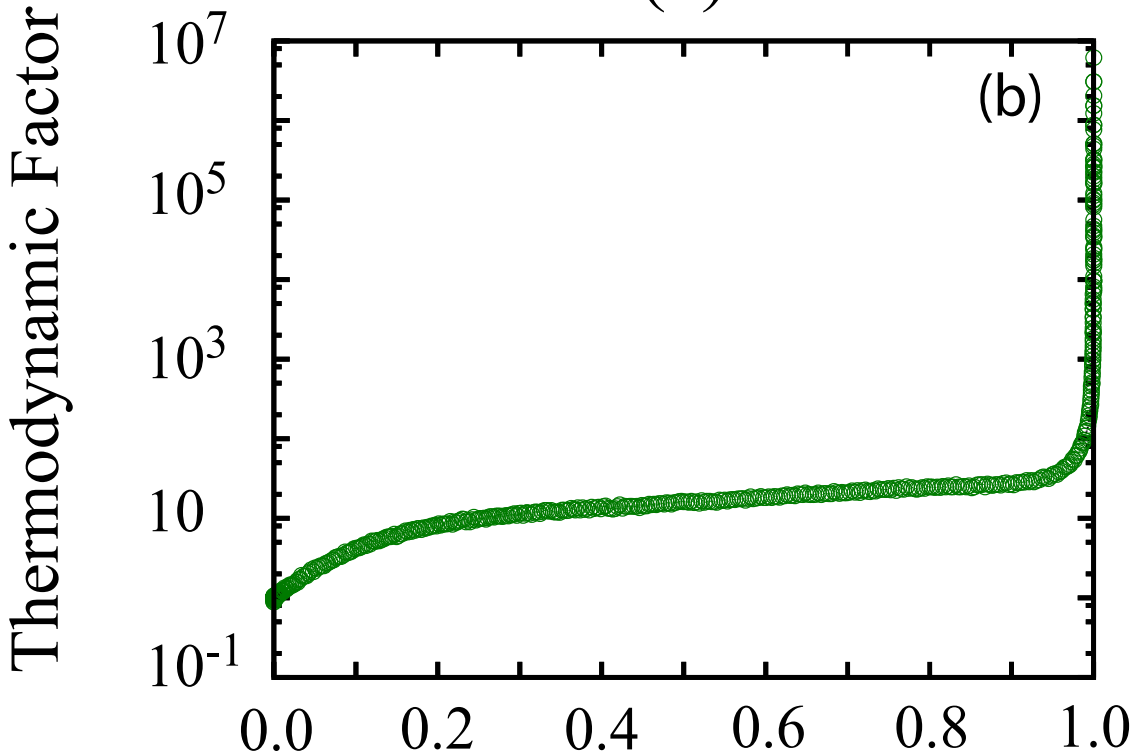

(b)

Figure 5 BY11342 03FEB2011

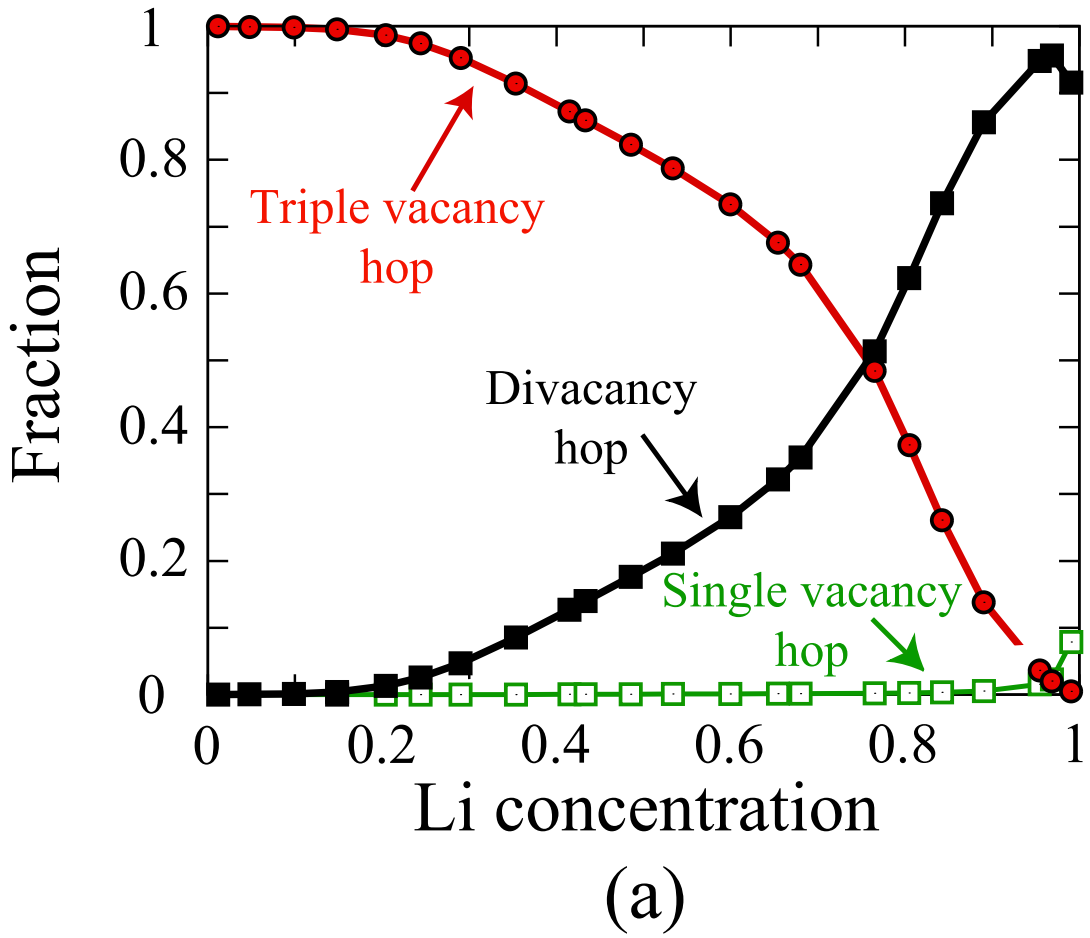

(a)

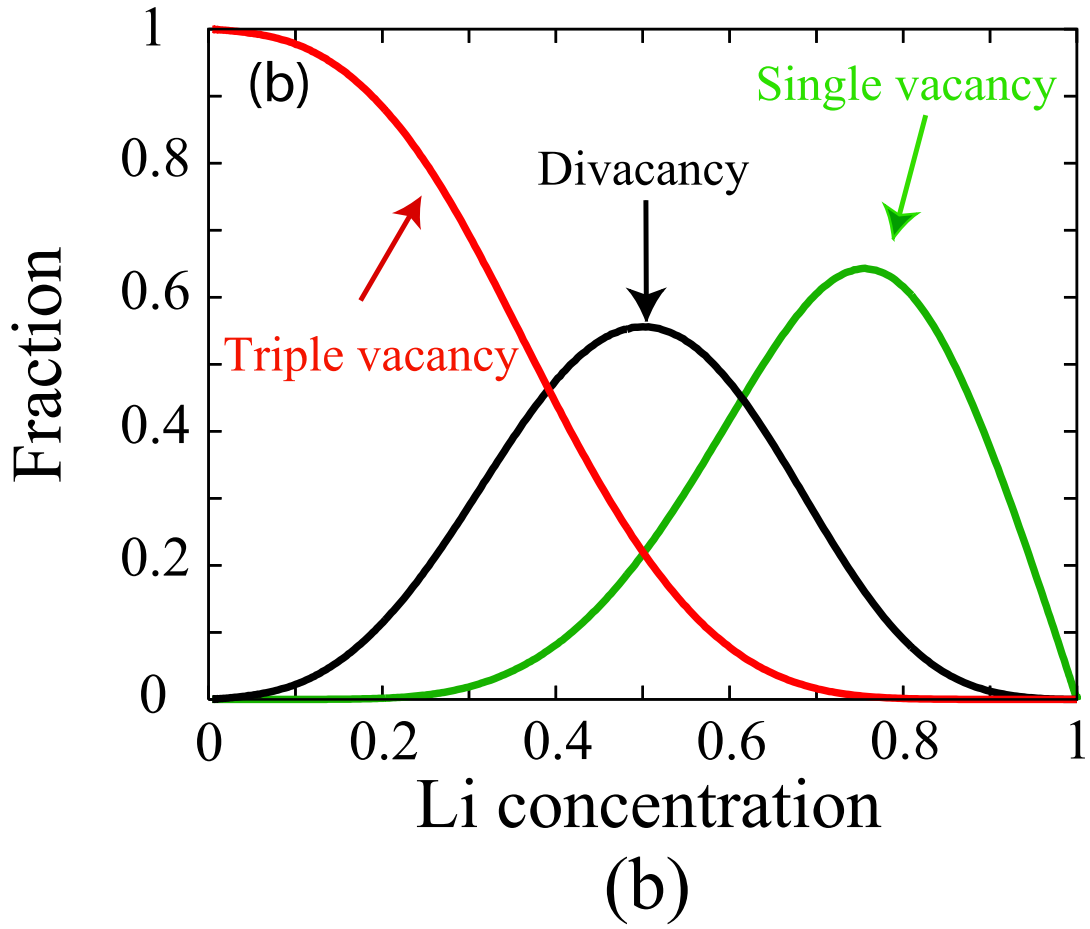

(b)

Figure 6 BY11342 03FEB2011

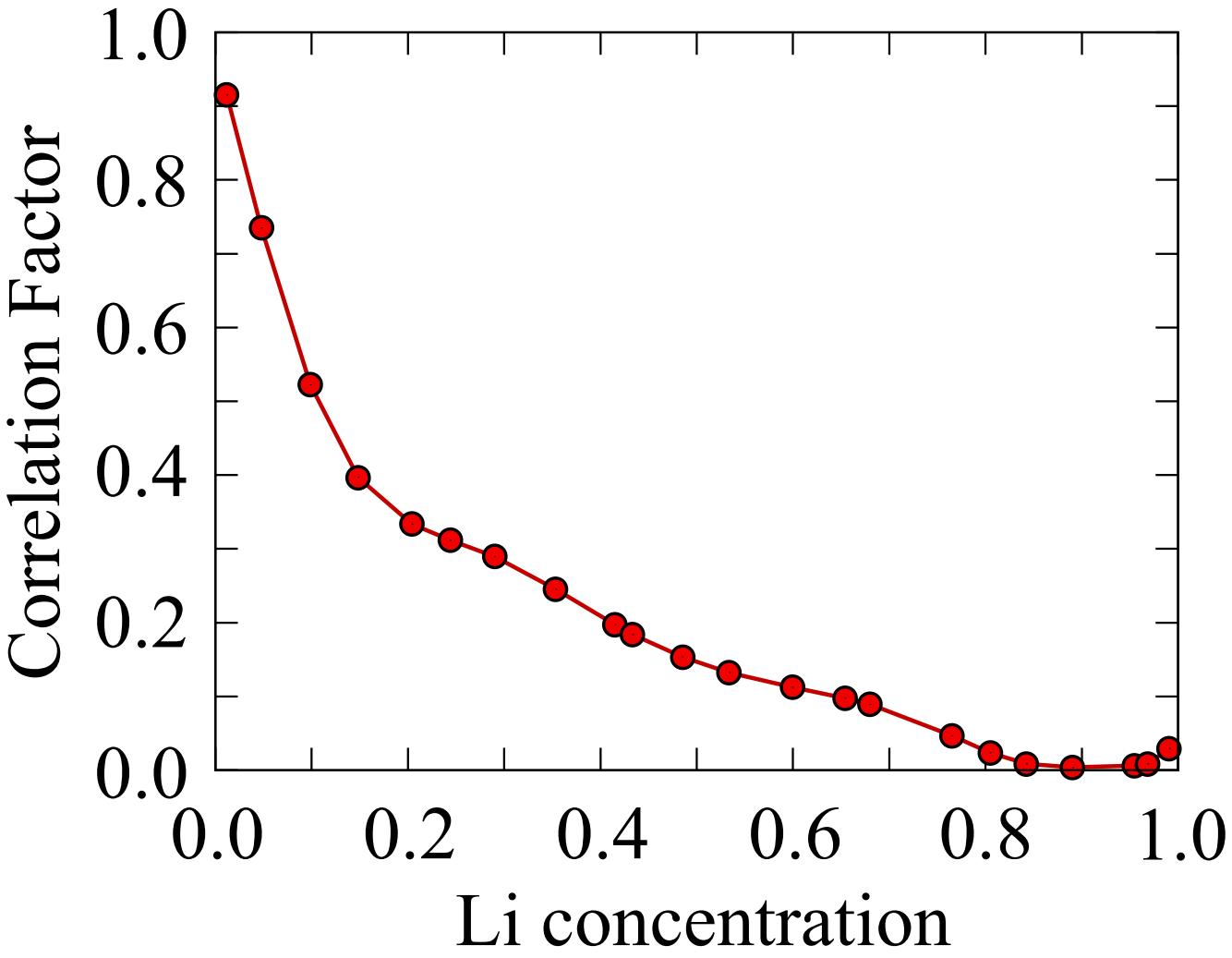

Figure 7 BY11342 03FEB2011